Supporting Information

for

Why does water in porous carbon generate electricity?: Electrokinetic role of proton in water droplet induced hydrovoltaic system of hydrophilic porous carbon

Hyunseok Ko, Wonkyeong Son, Min Sung Kang, Han Uk Lee, Chan-Yeup Chung, Seungwu Han, Changsoon Choi, Sung Beom Cho[*]

Dr. H. Ko, Dr. C. Chung,
Center of Materials Digitalization
Korea Institute of Ceramic Engineering and Technology
Jinju, Gyeongsang-namdo, 52851, Republic of Korea

W. Son, Prof. C. Choi
Department of Energy and Materials Engineering
Dongguk University-Seoul
Seoul, 04620, Republic of Korea

Prof. S. Han
Research Institute of Advanced Materials
Seoul National University
Seoul, 08826, Republic of Korea

Prof. S. Han
Department of Materials Science and Engineering
Seoul National University
Seoul, 08826, Republic of Korea

M. S. Kang, H. U. Lee Prof. S. B. Cho[*]
Department of Materials Science and Engineering
Department of Energy Systems Research
Ajou University
Suwon, 16499, Republic of Korea
*E-mail: csb@ajou.ac.kr

SI 1.   Domains of the FEM model

The physics used for hydrovoltaic model (Section 2 of the maintext) are applied to different domains. Here we show the construction of the model and how the domains are partitioned. The initial water droplet is given in the domain ①. The output voltage is measured by the electrostatic potential difference between the domain ② and ⑤. The Richard's equation and TDS is applied to all domains (①—⑤), while the chemical reaction and evaporation is applied to (②—⑤). The domain ③ and ④ are treated same, except for the investigation on effect of evaporation where the RH_t is set differently for ④ and ⑤.
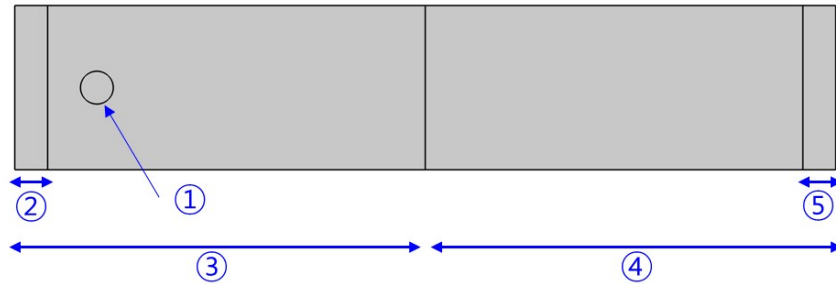

Fig. S. 1. The geometry and domains used in this study.

SI 2.   Retention model by Van Genuchten

The analytic formulas of van Genuchten[1] is frequently used for variably saturated flow modeling. The formulas are expressed in terms of pressure head, $H_P = p/(\rho g)$, and saturated and residual liquid volume fractions. The van Genuchten equations define saturation when the fluid pressure is atmospheric (that is, Hp = 0). With the parameters in Table 2, these equations are defined as:

$$\theta = \begin{cases} \theta_r + Se(\theta_s - \theta_r) & H_P < 0 \\ \theta_s & H_P \geq 0 \end{cases}$$

$$Se = \begin{cases} \left[1 + |\alpha H_P|^n\right]^{-m} & H_P < 0 \\ 1 & H_P \geq 0 \end{cases}$$

$$C_m = \begin{cases} \dfrac{\alpha m}{1-m}(\theta_s - \theta_r)Se^{-m}(1 - Se^{-m})^m & H_P < 0 \\ 0 & H_P \geq 0 \end{cases}$$

$$k_r = \begin{cases} Se^l[1 - (1 - Se^{-m})^m]^2 & H_P < 0 \\ 1 & H_P \geq 0 \end{cases}$$

here, α is the inverse of the air-entry matric potential which describes the capillary motion of the soil, as illustrated in Fig. S. 2. At very low matric potentials, the water menisci become disconnected and the soil is said to be at the 'residual' water content. Thus, the soil tends to maintain saturated state when α is greater, and capillary motion is promoted when α is smaller. Since the cotton fabrics are known for its high wettability, we have chosen a value, 1. 15 m^{-1}, lying at the lower bound of reported range of α (0.8 – 14.5 m^{-1}). The n and m are curve shape parameters, where n is a dimensionless coefficient related to the pore size distribution and has relation to Mualem coefficient of $m = 1 - (1/n)$. The soils are typically categorized by particle size as sand (2 – 0.05 mm), slit (0.05 – 0.002 mm), and clay (< 0.002 mm), and their n values are reported as 2.68, 1.37, and 1.09, respectively (decrease with particle size in general). Based on our FE-SEM analysis, the pores are in a scale of hundreds of micrometers, we have chosen n value of 2.03 which is the lower bound of sand.
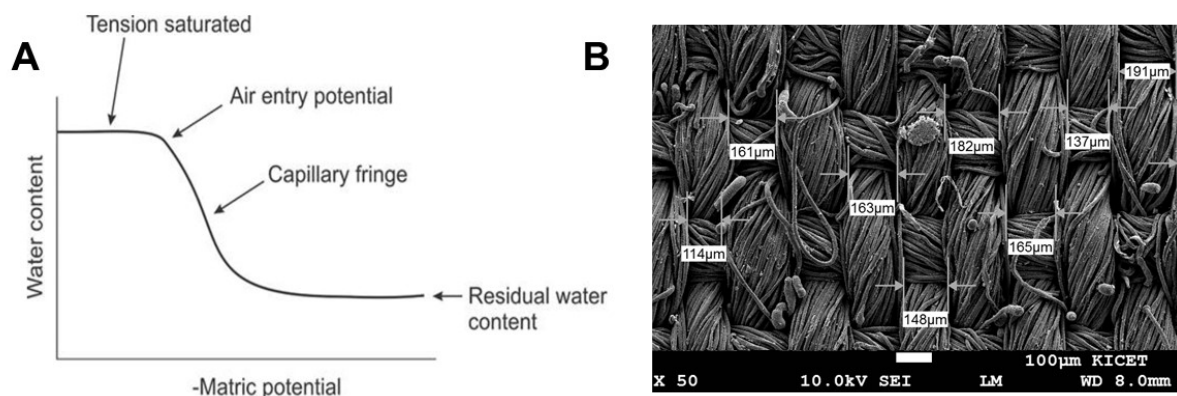
Fig. S. 2**. (A)** Ideal water release curve (retrieved from Ref [2]). **(B)** The FE-SEM image of CB coated fabric.

SI 3.   Analysis of surface chemical bonds

XPS analysis was performed to figure out functional groups formed on the surface of CB coated fabric. The peaks of hybridized carbon atoms were found at 284.2 (sp3) and 285.2 eV (sp2). The peaks of oxygen functional group were found at 286.2 (C-O), 287.5 (C=O), and 289.2 (COOH). Thus, it can be concluded that the surface bonds are dominantly hydroxyls as suggested by ref 37 in the main text.
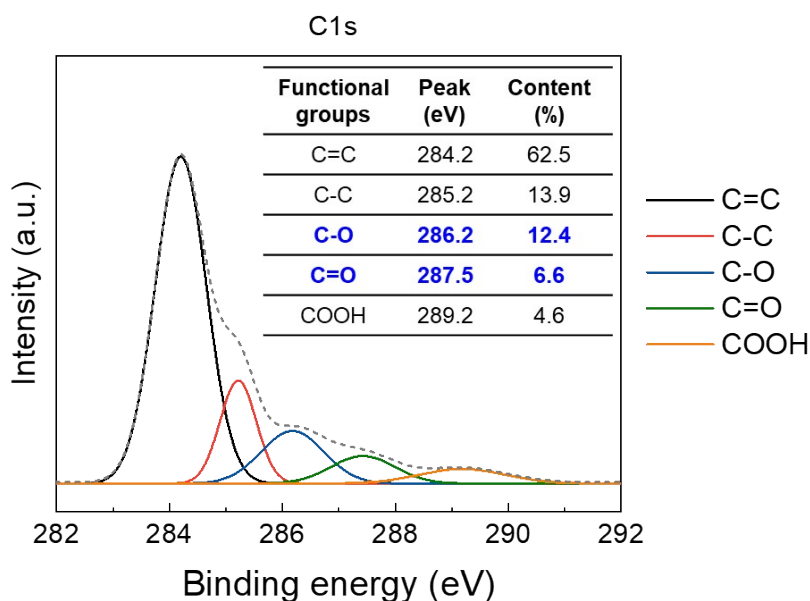

Fig. S. 3. C1s XPS spectra for CB coated fabric

SI 4.　　　Output power of the hydrovoltaics

The present study focused on elucidation of electricity generation; however, the current and output power are important values for energy harvesters. The measured the current and calculated power is shown in Fig. S. 4. The peak current of 2.3 μA is found at time where peak voltage is measured, and the current decays with increasing time. In similar study of water droplet on the CB film[3] also reported the peak current as few μA and the decaying propensity, which agree well with our measurements.
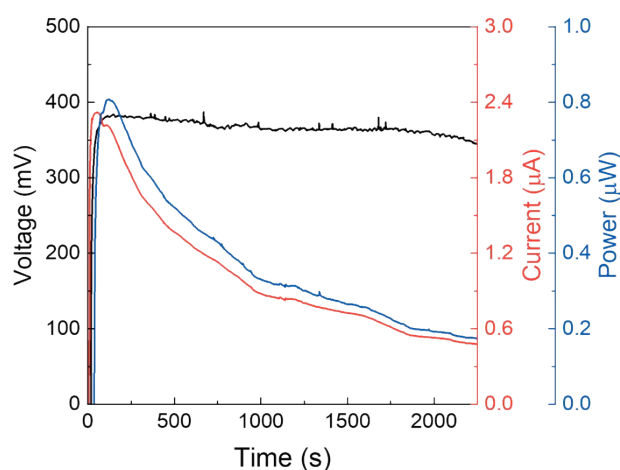

Fig. S. 4. Measured voltage (black), current (red), and power (blue) for hydrovoltaic system in this study.

SI 5.　　　Effect of chemistry

The protonation from the chemical reaction between water and substrate ($R2$) is an essence for the working principles of hydrovoltaic whose substrate is carbon-based or any other oxygen-containing surface functional groups, as ascribed in Figure 3. Hence, the reactivity of the surface, by means of catalysts or functionalized surfaces can greatly enhance the performance of the hydrovoltaic. We have adjusted the frequency factor for $R2$ (ω_{R2}) of Arrhenius reaction rate equation to investigate the effect of protonation. In Fig. S. 5A the voltage profiles are

depicted for cases with ω changed by a factor of two. The output voltages are found to be greater for cases with higher reaction rates and consequent higher net proton generation. The voltage linearly changed with the ω_{R2} value from the standard case of ω^0 ($V_{max.} = 380$ meV), where the $V_{max.}$ of ~530 and ~130 meV are captured for $0.5\omega^0$ and $2\omega^0$, respectively, showing a linear response to the change. The linear response is due to the change in overall H_3O^+ concentration, which can be seen by the quantitative analysis of the H_3O^+ flux shown in Fig. S. 5B. As ω_{R2} increase, the fluxes linearly increase for both diffusive (Φ_d, driven by concentration gradient) and electrophoretic fluxes (Φ_e, driven by charge gradient) but with opposite signs.
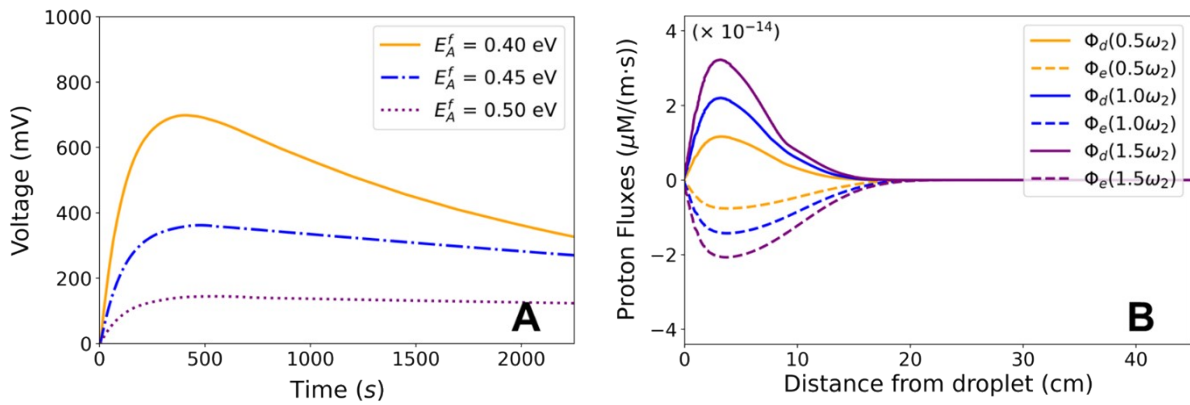

Fig. S. 5. Effect of the rate of the CB — Water chemical reaction on the hydrovoltaic model. (A) Output Voltages for CB surface with different chemical reaction rates (ω_2). (B) The diffusive proton flux (Φ_d) and electrostatic flux (Φ_e) at 660 s for different ω_2.

In this very first hydrovoltaic model, we aimed to build the most intrinsic case, and have used ion-free distilled water. It is worth mentioning that the co- presence of charged ions in water droplet will cause a change in the chemistry, although we have used an ion-free distillated water. For instance, Na^+ ions can be adsorbed on the $C=O^-$ surface functional, influencing electrostatic interaction across the CB film, as well as the protonation rate. In fact, the study

using sodium chloride solution has shown 40 % decreased performance than tap water[4], indicating that the process is sensitive to the ionic type and concentrations. Also, when the water droplet is not neutral in pH, the chemical reaction rates can be altered by shifted equilibrium. In Fig. S. 6 (a), the potential difference, which largely owes to H_3O^+ concentration, is diminished at acidic condition. The impact of pH on the maximum output is observed logarithmical as in Fig. S. 6 (b). The high H_3O^+ concentration in the droplet may enforced a stronger driving force for the saturation across the CB film. It should be pointed out that the co-ion effect needs to be considered in changed pH. Other anions are inevitably introduced in practice when changing the pH of the solution, while our initiative model currently does not account for co-ion effect.
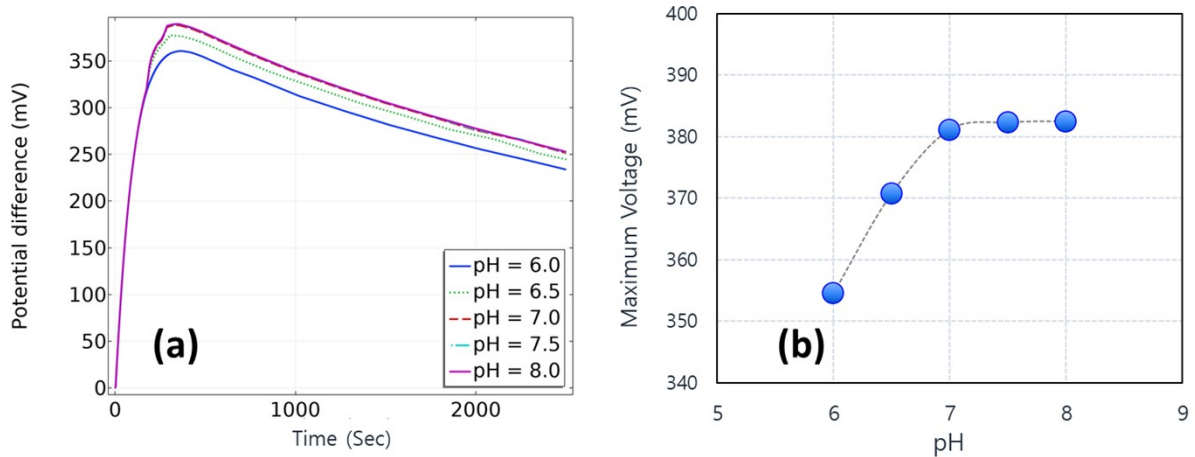

Fig. S. 6.   (a) The effect of initial pH of droplet on the voltage profile, and (b) the maximum voltage as a function of pH

SI 6.   Effect of porosity

Increased porosity of substrate makes it highly amendable for water molecules to transport through abundant channels and to vaporize into the surrounding air. For these reasons, studies were carried out to envisage highly porous substrates to maximize energy generation[5,6]. Herein, the effect of porosity is first investigated. The V_{oc} is smaller for higher ϵ_p as it can be seen from Fig. S. 7A. For high porosity ($\epsilon_p = 0.6$), the flow of water through porous medium is rather fast;

as shown in Fig. S. 7B and Fig. S. 7A, the c_{H_2O} is highly concentration near initial drop position after 350 s, while c_{H_2O} has diminished for higher porosity. The fast dispersion of water in high ϵ_p endows water to react with 'bare' surface (i.e., high c_{C-OH}), but at the same time, the evaporation is greater for high ϵ_p— the former promotes deprotonation, but the latter demotes deprotonation by decreasing c_{H_2O}. The c_{H_2O} distribution along x-direction at 350 s (Fig. S. 8B) shows that the net proton concentration is greater for lower ϵ_p. This infers that the suspension of water near the initial drop secures sufficient time for protonation reactions and, more importantly, slows down the evaporation, which can be confirmed with E_v at 350 s (Fig. S. 8C). At initial stage (< 300 s), the evaporation rates for all porosities are similar in scale near droplet. However, the evaporation is expedited for greater porosities when it becomes further from the droplet. In a regime where the water concentration is relatively low (x $>$ 20 cm), the evaporation rate is mostly greater for case with high porosity.
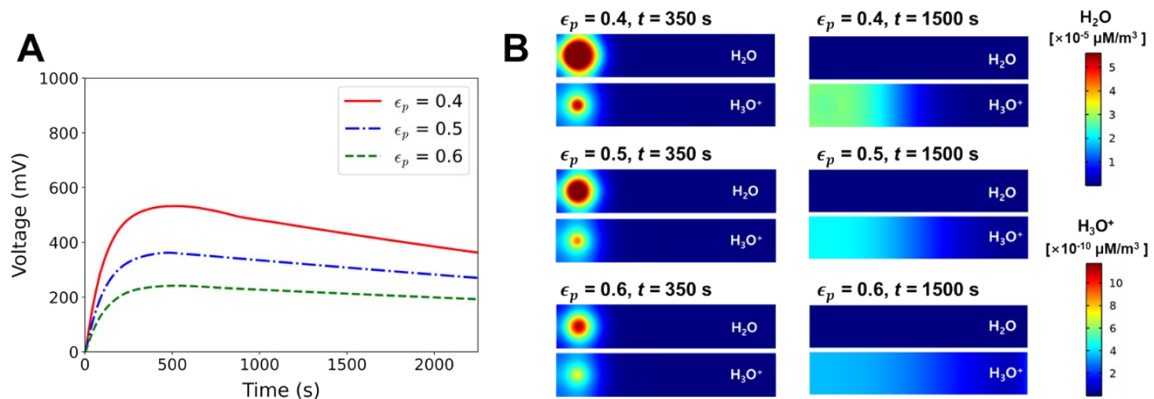

Fig. S. 7.   Effect of the porosity of the carbon black on hydrovoltaic model. **(A)** Output Voltages for CB with different porosities, and **(B)** the surface concentration gradient of H_2O and H_3O^+ are shown at 50 and 1500 seconds after water dropped.
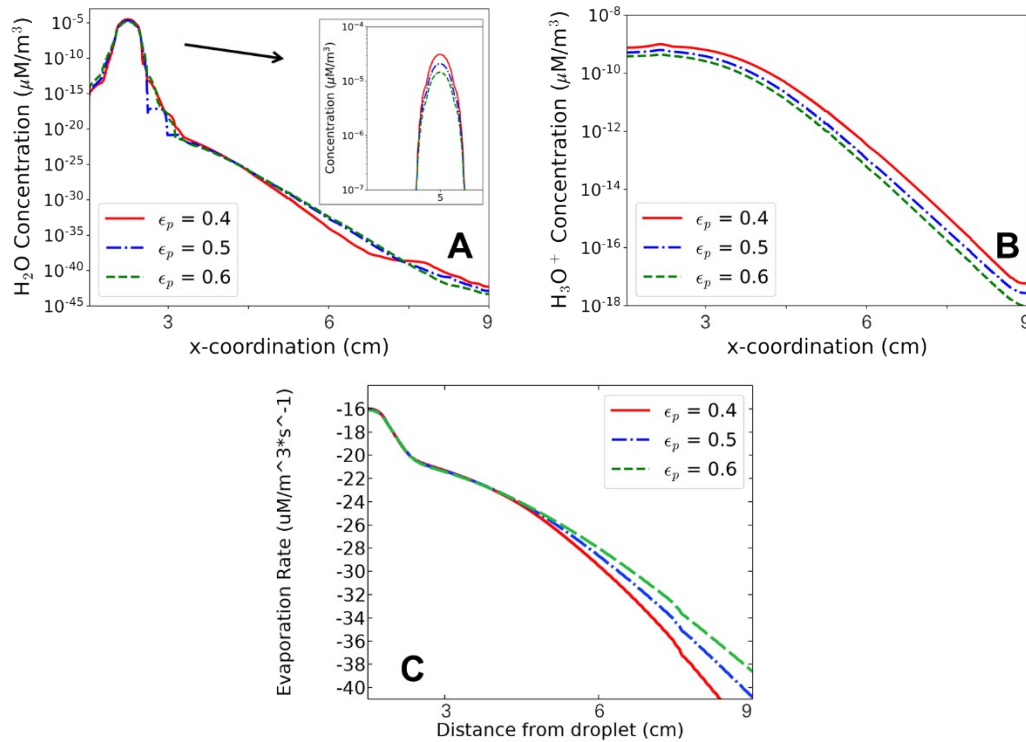
Fig. S. 8. The concentration distribution for **(A)** H_2O, and **(B)** H_3O^+, and **(C)** the evaporation rates in x-direction at 350 s.

The low c_{H_2O} of permeating front (equivalently low p_{VA}) expedite the evaporation as expressed in Eq. 5. At 1500 s, the gradient of c_{H_2O} is greater for low ϵ_p as the slower flow of water—permeation and evaporation. These observations suggest that the effect of porosity on the evaporation rate is greater than that on the flow-enhanced protonation reactions.

To date, the significance of porosity has been stressed in a number of studies, yet its effect is rarely investigated due to experimental difficulties. Here, for the first time, evaluated the effect of porosity which has an inversely proportional effect. With low ϵ_p, a slow but steady water flow (i.e., permeation and evaporation) develops higher V_{oc} and takes longer to reach maximum V_{oc}. It must be pointed out that a certain degree of porosity is essential for enabling working principles of hydrovoltaic generators. The lower porosity might be desired for improved performance, but without porosity or insufficient porosity will not allow transportation of

charged species and the solvent, water, and it is certainly not beneficial for the electric current. Another point that needs to be stressed is that the porosity and Richard's equation are taken as mean-field. The pore distribution (i.e., pore size, number density) is not precisely modeled, therefore the results are suggested for fundamental principles and should apply carefully to topological hydrovoltaic generators[7–11].

SI 7.   Effect of evaporation rate

The voltage output can be further improved by accelerating the evaporation rate, either by increasing temperature[7], increasing wind speed[12], placing external water absorption source[13] (e.g., desiccant), and decreasing humidity level[14,15]. In either method, the expedited evaporation rate promotes the flow of water/vapor through the substance and thereby generates electricity, as proven in a number of studies of maneuvering the local vaporization rates[3,12–14,16,17].

A transpiration mode was first designed, where the atmospheric RH for the tail of the substrate (RH_t) is set differently whereas the RH for the head (RH_h) was set to an ambient value of 60% at room temperature. The RH through the substrate is set linear, $RH(x) = RH_h + (RH_t - RH_h) * \frac{x}{lx}$. In Fig. S. 9A, the effect of RH_t on the output voltage is shown. For the lower RH_t (i.e., drier atmosphere), the evaporation on the tail is stimulated thus the gradient of water concentration becomes greater and promotes water flow toward the tail for replenishment (Fig. S. 9B). The dissipation of water becomes more rapid in $+x$ direction. At the same time, the protonation reaction with CB films (*R2*) occurs on a greater scale, as the dispersed water molecules encounter 'fresh' CB films with higher C-OH concentrations. Up to this point, the low RH_t case has similarities with high ϵ_p (Fig. S. 7), where the water flow is accelerated towards the tail in both cases. Yet, the difference is the localization of evaporation. The E_v gradually increase

towards the tail ensuring a relatively sufficient time for protonation in low RH_t, unlike high ϵ_p case. The increased E_v is global in high ϵ_p and less water attributes to protonation and transport of ions. Thus, the $R2$ is promoted as the water advance in $+x$ direction, as shown in Fig. S. 10. On the other hand, for higher RH_t, the water relatively stagnates from the initial droplet. The water evaporates even at high humidity, as the vapor pressure above the droplet is always higher than the ambient vapor pressure. Thus, the water near the droplet evaporates more before propagating towards the tail compared to the case of low RH_t. Therefore, the protonation is limited to the area near the droplet, and overall generated $c_{H_3O^+}$ is lower. For the same reason, the voltage profile under dry circumstances ($RH_t = 30\%$) reaches the maximum slower than the humid condition ($RH_t = 90\%$), as the higher $c_{H_3O^+}$ takes a longer time to find equilibrium (Fig. S. 11).
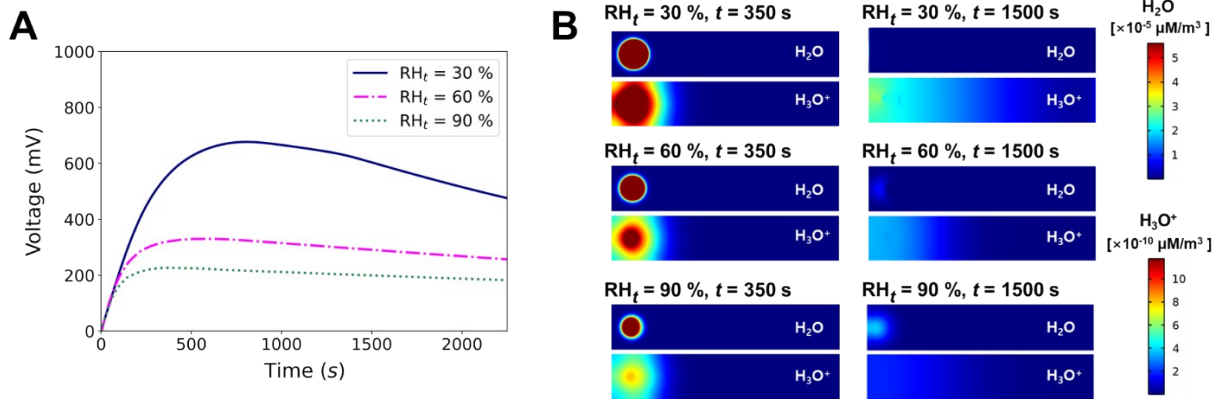

Fig. S. 9. Effect of the rate of the relative humidity applied on the right-half of the CB (RH_t). **(A)** Output Voltages for different evaporation rate (right-half) depending on the RH, and **(B)** the surface concentration gradient of H_2O and H_3O^+ are shown at $t = 350$ and $t = 1500$ s after water dropped.
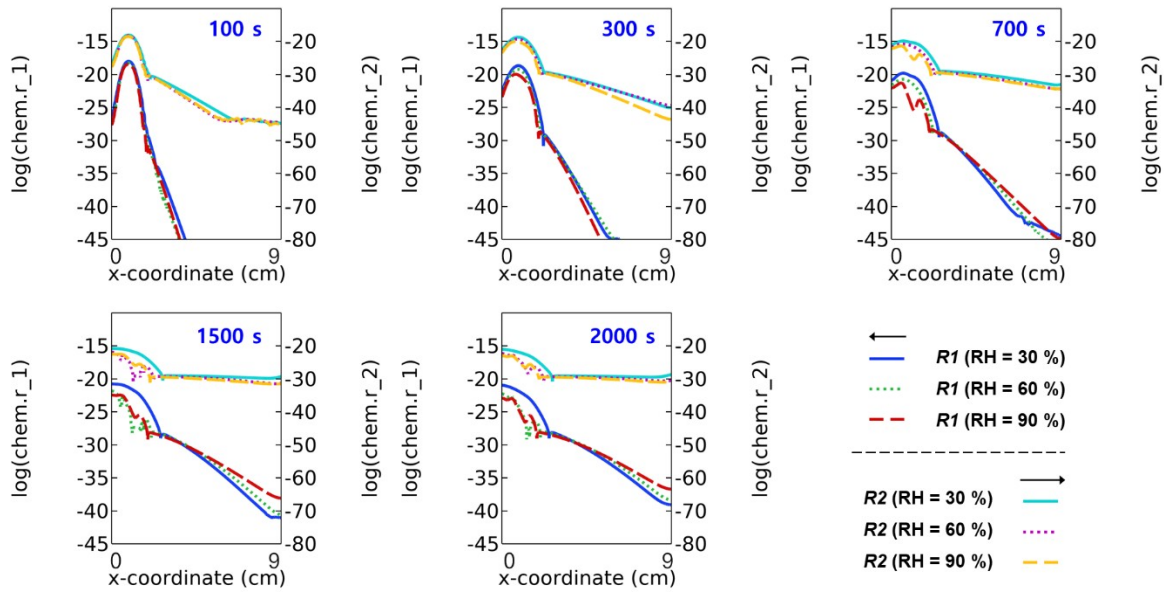
Fig. S. 10. The reaction rates (R1 and R2) for different RH values at different time steps.
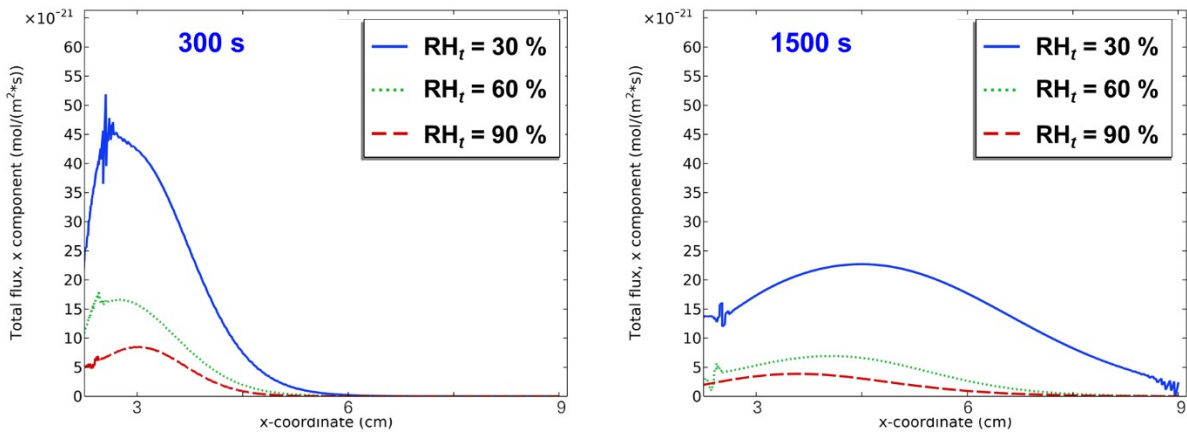

Fig. S. 11. The proton flux for different RH values at different time steps.

SI 8.   Effect of geometry

The essence of hydrovoltaic is the proton gradient induced by generation from surface reactions combined with the gradient in water molecule density (moisture), as explained earlier. Thus, the geometry of CB possibly can affect the output voltage by maneuvering the degree of local

chemistry and dynamics. For the amount of water used in this study, however, the size of CB film is "sufficiently small", thus V_{oc} almost always decrease with increasing dimensions (i.e., the overall proton concentration becomes dilute). To understand the geometric effect, we have simulated similar case in a larger-scale CB film of 10 cm × 50 cm.

To do so, we designed CB films in different isosceles trapezoid shapes (10, 20, 30, and 40 cm). In terms of the output voltage, it was discovered that it is a competing effect between the width of CB film near droplet and surface area (*area-to-wet*, S_{CB}) and proton gradient. Here we define *a* as the length of the CB film near the water source, whereas *b* is the length of the other side (tail).

For smaller *a*, the ions can be concentrated on the head due to the small area to wet, but for larger *a,* the ions become diluted on the head. Therefore, as displayed in Fig. S. 12A, the voltage is found greater for smaller *a*. The maximum V_{oc} achieved for each *a* showed a strong dependency on *a*, although it depends on *b* values as well. In the inset of Fig. S. 12A, the pairing *b* values are shown, as well as the $c_{H_3O^+}$ distribution at the time where maximum V_{oc} is observed. For each maximum voltage cases, the *b* tends to decrease as *a* increases, and this is because S_{CB} becomes too large when both *a* and *b* are large, resulting in a spread concentration of H_3O^+ over the film. As the color scale shows, the proton concentration at the head is diluted as *a* value increases. In Fig. S. 12B, we have investigated the effect of the overall surface area for a given value of *a*. For each *a* (Fig. S. 13), we found that there is an optimal surface area to give the highest output, showing a 'volcano' type relation. For *a* = 10 cm, when the surface area is not too large ($\leq$ 1000 cm^2), voltage values from isosceles trapezoid CB films are greater than that of a traditional rectangle CB film (= 500 cm^2) with the identical microstructure. However, when S_{CB} is too large (> 1000 cm^2), the overall concentration is diluted and

decreases V_{OC}. Despite the difference in the area for maximum V_{OC}, identical trends are found for other values of a as well (Fig. S. 12). In short, the larger S_{CB} results in lower ion concentration in general, but the narrower S_{CB} diminishes the concentration difference due to saturation.

This result indicates that both the total surface area and the surface area near the droplet impose significance for the output voltage. This is consistent with the argument from a similar study of immersion (although the hydraulic dynamics can be quite different as the source of water is quantitatively and timely different) where it was claimed that the devices with different shapes show not only different outputs but also different design rules[18]. The result is intriguing that there are many possible scenarios: the loading type (water droplet or water immersion or moisture) and loading amount can lead to a different governing physics. Our results suggests that the effect of length a and area of CB film can be different for system with different ratio of water droplet volume to dimension of CB film. Furthermore, the length a is less important for immersion case, as there is a semi-infinite source of water, thus only thing matters are the S_{CB}. On the other hand, for the cases of limited water source as vapor in the air, the length a plays more significant role as it determines the difference in local water vapor concentration between the head and tail.
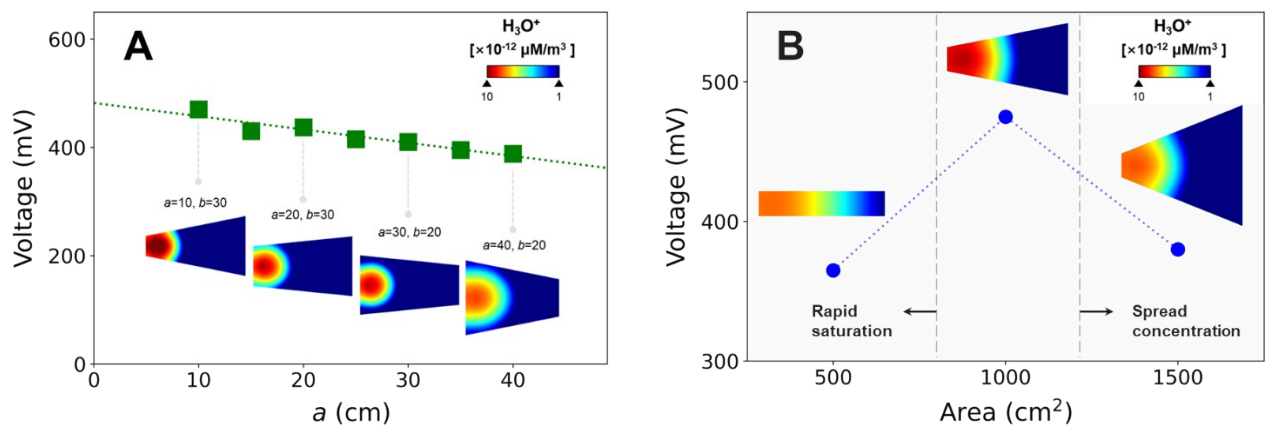
Fig. S. 12. The effect of the geometric change on the voltages. **(A)** the maximum voltage achieved for each a (while varying b with interval of 5 cm). A higher V_{oc} output is found for smaller a. The surface plots show H_3O^+ distribution at $t = 1500$ s. **(B)** The effect of total area on voltages for cases with $a = 10$ cm (note that the "inverse V" relation hold for other a values.) The surface plots illustrate the H_3O^+ concentration on each geometry at $t = 1500$ s.
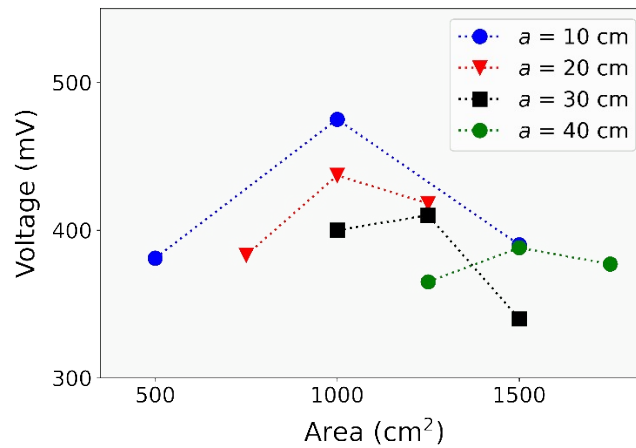

Fig. S. 13. The areal dependency of voltage outputs for different a values.

SI 9.   Model modification: Water immersion

The dropcasting and other system(dipping) can be driven by different mechanism depending on the architecture of system and water source, but the essential physics are common; it is matter of which physics governs the most. To verify, we have used very same model for the case when one-end is dipped in the water. While the model system is not particularly optimized for water circulation (e.g., control of pore structure or presence of desiccant), we found that the voltage is maintained over 30 days.
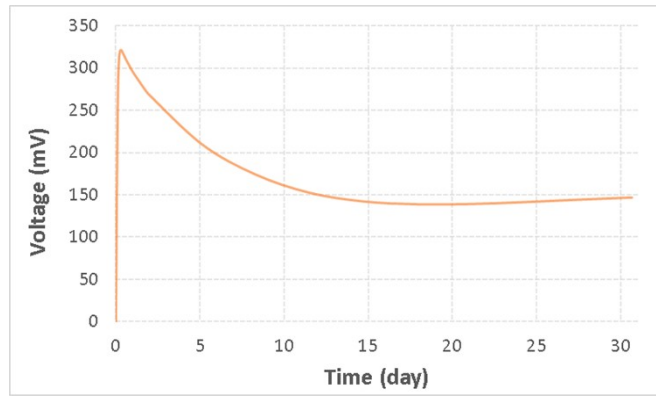
Fig. S. 14 Voltage profile of immersion hydrovoltaics system

SI 10.   **Current loop**

It is generally acknowledged that the detailed mechanism for current loop formation is not clearly understood. For example, the flow of ions in the fluidic channel will lead to the external electronic current which requires the redox process generally. To understand this behavior, we further analyzed this current generation behavior. In order to prevent any unexpected effect for electrochemical measurement, the CB sheet is directly connected to the zig of a working electrode of the electrochemical analyzer (Vertex, I-vium tech, Netherland) in the three-electrode system. In most experiments, therefore, no redox peaks, gas bubbling, or electrochemical reactions were observed. This is consistent with the previous report on the moisture-induced electricity generation.[19] This electronic current production without redox can be understood with 'image charge' model. The voltage generation and ionic flow by the water will induce the electric field inside the channel material, and the mobile electrons of the channel materials will flow and form the current loop. We believe such a current loop can be sustained by proton backflow and recombination of the functional groups with looped-backed electrons from the channel material. Firstly, when the proton across the carbon is saturated, the driving force from diffusive flux becomes nearly 0. Then the electrophoretic flux derives the proton flux in reversed direction (from right to left in the model). The electrons from the current loop meet this backflowed protons, diminishing the initial proton gradient. In open-circuit condition, the reverse reaction of natural decomposition of water can also allows the replenishment of H_2O and endow a continuous current generation. Hence, the voltage output vanishes as the all the functional group recombined and proton gradients converges to zero.

References

1. Genuchten, M. Th. van. A Closed-form Equation for Predicting the Hydraulic Conductivity of Unsaturated Soils. *Soil Sci Soc Am J* 44, 892–898 (1980).

2. Whalley, W. R., Ober, E. S. & Jenkins, M. Measurement of the matric potential of soil water in the rhizosphere. *J. Exp. Bot.* 64, 3951–3963 (2013).

3. Yun, T. G., Bae, J., Rothschild, A. & Kim, I.-D. Transpiration Driven Electrokinetic Power Generator. *Acs Nano* 13, 12703–12709 (2019).

4. Zhu, G. *et al.* Harvesting Water Wave Energy by Asymmetric Screening of Electrostatic Charges on a Nanostructured Hydrophobic Thin-Film Surface. *Acs Nano* 8, 6031–6037 (2014).

5. Zhao, F., Liang, Y., Cheng, H., Jiang, L. & Qu, L. Highly efficient moisture-enabled electricity generation from graphene oxide frameworks. *Energ. Environ. Sci.* 9, 912–916 (2016).

6. Zhao, F., Cheng, H., Zhang, Z., Jiang, L. & Qu, L. Direct Power Generation from a Graphene Oxide Film under Moisture. *Adv. Mater.* 27, 4351–4357 (2015).

7. Shao, B. *et al.* Bioinspired Hierarchical Nanofabric Electrode for Silicon Hydrovoltaic Device with Record Power Output. *Acs Nano* 15, 7472–7481 (2021).

8. Huang, Y. *et al.* Interface-mediated hygroelectric generator with an output voltage approaching 1.5 volts. *Nat. Commun.* 9, 4166 (2018).

9. Nie, X. *et al.* Gradient doped polymer nanowire for moistelectric nanogenerator. *Nano Energy* 46, 297–304 (2018).

10. Qin, Y. *et al.* Constant Electricity Generation in Nanostructured Silicon by Evaporation-Driven Water Flow. *Angew. Chem. Int. Ed.* 59, 10619–10625 (2020).

11. Zhao, X. *et al.* A Simple High Power, Fast Response Streaming Potential/Current-Based Electric Nanogenerator Using a Layer of Al2O3 Nanoparticles. *Acs Appl Mater Inter* 13, 27169–27178 (2021).

12. Ding, T. *et al.* All-Printed Porous Carbon Film for Electricity Generation from Evaporation-Driven Water Flow. *Adv. Funct. Mater.* 27, 1700551 (2017).

13. Bae, J., Yun, T. G., Suh, B. L., Kim, J. & Kim, I.-D. Self-operating transpiration-driven electrokinetic power generator with an artificial hydrological cycle. *Energ. Environ. Sci.* 13, 527–534 (2020).

14. Xue, G. *et al.* Water-evaporation-induced electricity with nanostructured carbon materials. *Nat Nanotechnol* 12, 317–321 (2017).

15. Li, C., Liu, K., Liu, H., Yang, B. & Hu, X. Capillary driven electrokinetic generator for environmental energy harvesting. *Mater. Res. Bull.* 90, 81–86 (2017).

16. Zhang, S., Chu, W., Li, L. & Guo, W. Voltage Distribution in Porous Carbon Black Films Induced by Water Evaporation. *J. Phys. Chem. C* 125, 8959–8964 (2021).

17. Yoon, S. G. *et al.* Natural Evaporation-Driven Ionovoltaic Electricity Generation. *Acs Appl Electron Mater* 1, 1746–1751 (2019).

18. Zhang, S., Fang, S., Li, L. & Guo, W. Geometry effect on water-evaporation-induced voltage in porous carbon black film. *Sci China Technological Sci* 64, 629–634 (2021).

19. Liu, X. *et al.* Microbial biofilms for electricity generation from water evaporation and power to wearables. *Nat Commun* 13, 4369 (2022).